ACADEMIC PRESS

Available online at www.sciencedirect.com

SCIENCE DIRECT®

Journal of Sound and Vibration 261 (2003) 329–349

JOURNAL OF SOUND AND VIBRATION

www.elsevier.com/locate/jsvi

Moving force identification based on the frequency–time domain method

L. Yu, Tommy H.T. Chan*

Department of Civil and Structural Engineering, The Hong Kong Polytechnic University, Hung Hom, Kowloon, Hong Kong

Received 5 September 2000; accepted 27 May 2002

Abstract

This paper addresses the problem on the identification of moving vehicle axle loads based on measured bridge responses using a frequency–time domain method. The focus is on the evaluation of two solutions to the overdetermined set of equations established as part of the identification method. The two solutions are (i) direct calculation of the pseudo-inverse and (ii) calculation of the pseudo-inverse via the singular value decomposition (SVD) technique. For this purpose, a bridge–vehicle system model was fabricated in the laboratory and the bending moment responses of bridge model were measured as a two-axle vehicle model moved across the bridge deck. The moving axle loads are then calculated from the measured responses via the two solutions to the over-determined set of equations. The effects of changes in the bridge–vehicle system, measurement and algorithm parameters on the two solutions are evaluated. Case studies show that the moving force identification is more feasible and its accuracy acceptable with the use of the SVD technique. This technique can effectively enhance the identification method and improve the identification accuracy over that of the direct pseudo-inverse solution.

1. Introduction

Accurate identification of moving forces in a bridge–vehicle system is an important issue from the aspects of design, diagnosis and maintenance of bridges. The indirect force calculation is of special interest when the moving wheel forces cannot be measured directly while the bridge responses caused by the moving vehicles can be measured easily [1,2].

Moving force identification has been studied extensively in recent years. A comprehensive survey of the references and methods for solving the problems involving moving loads on

*Corresponding author. Tel.: +852-2766-6061; fax: +852-2334-6389.
E-mail address: cetommy@polyu.edu.hk (T.H.T. Chan).

0022-460X/03/$ - see front matter
PII: S0022-460X(02)00991-4

structures can be found in Fryba's book [3]. The original "moving-mass moving-force" problem was approximated by the simplified "moving-force" problem by Timoshenko et al. [4]. In this field, the authors have successively proposed four identification methods, in which the interpretive method I (IMI) [5] calculated the moving dynamic forces directly by modelling a bridge as an assembly of lumped masses interconnected by massless elastic beam elements. Time domain method (TDM) [6] modelled the forces on a simply supported Euler beam as step functions in a small time interval and identified the forces by using the modal superposition principle in time domain. Frequency–time domain method (FTDM) [7] performed Fourier transformation on the equation of motion that was expressed in modal co-ordinates. The relation between the responses and the forces was obtained in frequency domain. The time histories of the forces were found by the least-squares method. Interpretive method II (IMII) [8] identified the forces completely in the modal co-ordinates by using the Euler beam theory and modal analysis technique.

Further comparative studies [9–11] showed that each of the four methods could effectively identify moving forces with acceptable accuracy to some extent but with some limitations. In particular, the identification method gives poor results and sometimes even incorrect estimate of moving forces in some situations. Insufficient accuracy of the measured data, ill conditioning of the mobility matrix, lack of proper consideration of the participation of the structural modes, and insufficient measurement locations are some of the reasons for poor accuracy of the force determination in a number of applications [12]. In addition, different ways to solve the equations are another important reason [13]. This is mainly because elements of *pseudo-inverse* (PI) matrices are sensitive to small perturbations in the data with noise, or say small perturbations in the data can yield large perturbations in the computed PI. In this sense, the singular value decomposition (SVD) can be thought of as a filter that provides a signal estimate from noise data [14]. The SVD technique, applied to structural dynamics problems in the last 35 years [15–17], is one of the most important tools in numerical analysis and widely used in the identification problem [18].

This paper concentrates on the evaluation of two different solutions to the overdetermined equations established in the FTDM. The two solution methods are (i) direct calculation of the PI and (ii) adopting the SVD technique to calculate the PI of the coefficient matrix in the over-determined equations. This paper first outlines the FTDM method and the laboratory experiments are then introduced. Case studies on the effects of various parameters on the two solutions are finally used to illustrate the practical aspects of the two solutions.

2. Basic theory

2.1. Equation of motion

Referring to Fig. 1, consider a force P moving from left to right at a speed c on a simply supported bridge deck with a span length L, constant flexural stiffness EI, constant mass per unit length ρ and viscous proportional damping C. The bridge deck is modelled as an Euler beam [3], and the differential equation on the deflection of the beam can be expressed as

$$\rho\frac{\partial^2 v(x,t)}{\partial t^2} + C\frac{\partial v(x,t)}{\partial t} + EI\frac{\partial^4 v(x,t)}{\partial x^4} = \delta(x-ct)P(t), \tag{1}$$

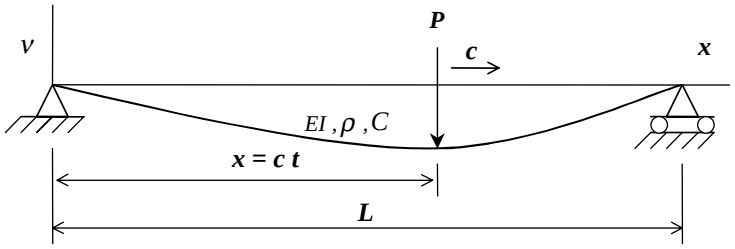

Fig. 1. Moving force on a simply supported beam.

where $v(x,t)$ is the beam deflection at point x and time t, $P(t)$ is the time-varying point force, E is Young's modulus of the beam, I is the second moment of inertia of the beam cross-section, and $\delta(x)$ is the Dirac delta function. Based on modal superposition, if the nth mode shape function of the beam $\Phi_n(x) = \sin(n\pi x/L)$, the solution of Eq. (1) is obtained as

$$v(x,t) = \sum_{n=1}^{\infty} \sin\frac{n\pi x}{L} q_n(t), \tag{2}$$

where n is the mode number (MN), $q_n(t)$, $(n = 1, 2, \ldots, \infty)$ are the nth modal displacements. After substituting Eq. (2) into Eq. (1), integrating the resultant equation with respect to x between 0 and L, and then using the boundary conditions and the properties of the Dirac delta function, the equation of motion in terms of the modal displacement $q_n(t)$ is given as

$$\frac{\mathrm{d}^2 q_n(t)}{\mathrm{d}t^2} + 2\xi_n\omega_n\frac{\mathrm{d}q_n(t)}{\mathrm{d}t} + \omega_n^2 q_n(t) = \frac{2}{\rho L} p_n(t) \quad (n = 1, 2, \ldots, \infty), \tag{3}$$

where

$$\omega_n = \frac{n^2\pi^2}{L^2}\sqrt{\frac{EI}{\rho}}, \qquad \xi_n = \frac{C}{2\rho\omega_n}, \qquad p_n(t) = P(t)\sin\left(\frac{n\pi ct}{L}\right) \tag{4}$$

are the nth modal frequency, the modal damping and the modal force, respectively.

Performing the fast Fourier transform (FFT) on Eq. (3), the Fourier transform of the dynamic deflection $v(x,t)$ is obtained as

$$V(x,\omega) = \sum_{n=1}^{\infty} \frac{1}{M_n}\Phi_n(x)H_n(\omega)P_n(\omega), \tag{5}$$

where $M_n = \rho L/2$, $H_n(\omega)$ is the frequency response function of the nth mode, and

$$H_n(\omega) = \frac{1}{\omega_n^2 - \omega^2 + \mathrm{i}2\xi_n\omega_n\omega}, \tag{6}$$

$$\Phi_n(x) = \sin(n\pi x/L), \tag{7}$$

$$P_n(\omega) = \frac{1}{2\pi}\int_{-\infty}^{\infty} p_n(t)\mathrm{e}^{-\mathrm{i}\omega t}\,\mathrm{d}t. \tag{8}$$

2.2. Force identification from accelerations

The Fourier transform of the acceleration of the beam at point x is obtained from Eq. (5) as

$$\ddot{V}(x,\omega) = -\omega^2 \sum_{n=1}^{\infty} \frac{1}{M_n} \Phi_n(x) H_n(\omega) P_n(\omega). \tag{9}$$

Substituting Eqs. (6)–(8) into Eq. (9) and rewriting in discrete terms,

$$\ddot{V}(m) = -\sum_{k=0}^{N-1} \sum_{n=1}^{\infty} \frac{\Delta f^3 m^2}{M_n} \Phi_n(x) H_n(m) \Psi_n(m-k) F(k), \quad m = 0, 1, \ldots, N-1, \tag{10}$$

where Ψ_n and F are the Fourier transform of the nth mode shape and the moving force $P(t)$ respectively. Δf is the frequency resolution, N is the number of data samples, k and m denote the kth and the mth term in the FFT, respectively. Considering the periodic property of the discrete fourier transform (DFT), then Eq. (10) can be rewritten in matrix form

$$\ddot{V}_{(N+2)\times 1} = A_{(N+2)\times(N+2)} F_{(N+2)\times 1}, \tag{11}$$

where $\ddot{V}$ and F are Fourier transform of the acceleration vector $\ddot{v}$ and the force vector $P(t)$, respectively. The matrix A is associated with the bridge–vehicle system. Dividing F into real and imaginary parts, F_R and F_I, respectively, Eq. (11) becomes

$$\ddot{V} = (A_{RR} + \mathrm{i}A_{RI})F_R + \mathrm{i}(A_{IR} + \mathrm{i}A_{II})F_I. \tag{12}$$

Dividing $\ddot{V}$ into real and imaginary parts $\ddot{V}_R$ and $\ddot{V}_I$, Eq. (12) can be rewritten in the form of the real and imaginary parts as

$$\begin{Bmatrix} \ddot{V}_R \\ \ddot{V}_I \end{Bmatrix}_{(N+2)\times 1} = \begin{bmatrix} A_{RR} & -A_{II} \\ A_{RI} & A_{IR} \end{bmatrix}_{(N+2)\times(N+2)} \begin{Bmatrix} F_R \\ F_I \end{Bmatrix}_{(N+2)\times 1}. \tag{13}$$

Since the first and last elements of the Fourier transform of the imaginary parts of vectors $\ddot{v}$ and P are equal to zero, i.e., $\ddot{V}_I(0) = \ddot{V}_I(N/2) = 0$, $F_I(0) = F_I(N/2) = 0$, Eq. (13) can then be condensed into a set of Nth order simultaneous equations by deleting corresponding rows and columns as

$$\ddot{V}_{RI(N\times 1)} = A_{C(N\times N)} F_{RI(N\times 1)}, \tag{14}$$

where $\ddot{V}_{RI}$ consists of components $\ddot{V}_R$ and $\ddot{V}_I$. F_{RI} consists of F_R and F_I, which can be found from Eq. (14) by solving the N order linear equations. The time history of the moving force $P(t)$ can then be obtained by performing the inverse Fourier transformation. However, for the general case when $N > N_B$, where $N_B = L/(c\Delta t)$, Δt is the sampling time interval, the identified force in the time interval $(N - N_B)\Delta t$ must be equal to zero when the response is not polluted by noise. Otherwise, a non-zero force identified in this interval would be meaningless. Furthermore, the computation cost for solving Eq. (14) is high in finding the inverse of a full matrix, and therefore the following procedure is developed to overcome these difficulties.

If the DFTs are expressed in matrix form, the Fourier transform of the force vector F will be written as follows:

$$F = \frac{1}{N} WP, \tag{15}$$

where $W = \mathrm{e}^{-\mathrm{i}2k\pi/N}$ and all terms in F are real.

$$k = \begin{bmatrix} 0 & 0 & 0 & \cdots & 0 & 0 \\ 0 & 1 & 2 & \cdots & N-2 & N-1 \\ 0 & 2 & 4 & \cdots & N-4 & N-2 \\ \vdots & \vdots & \vdots & \ddots & \vdots & \vdots \\ 0 & N-2 & N-4 & \cdots & 4 & 2 \\ 0 & N-1 & N-2 & \cdots & 2 & 1 \end{bmatrix}_{N\times N}. \tag{16}$$

The matrix W is an unitary matrix, which means

$$W^{-1} = (W^*)^{\mathrm{T}}, \tag{17}$$

where W^* is the conjugate of W. Substituting Eq. (15) into Eq. (14), yields

$$\ddot{V} = \frac{1}{N} A \underset{N\times N_B}{[W_B\ 0]} \begin{Bmatrix} P_B \\ 0 \end{Bmatrix}, \tag{18}$$

or

$$\underset{N\times 1}{\ddot{V}} = \frac{1}{N} \underset{N\times N}{A}\ \underset{N\times N_B}{W_B}\ \underset{N_B\times 1}{P_B}, \tag{19}$$

linking the Fourier transform of acceleration $\ddot{v}$ with the force vector P_B of the moving forces in the time domain. W_B andP_B are the sub-matrices of W and P, respectively. Using Eq. (19) for identification has the advantage of weighting the response data in the frequency domain, but the disadvantage is that the noise of the responses during the time interval $(N_B\Delta t)$ to $(N\Delta t)$ will affect the accuracy of the identified forces. Eq. (19) can be written using Eq. (15) to relate the accelerations and force vectors in the time domain as

$$\underset{N\times 1}{\ddot{v}} = \underset{N\times N}{(W^*)^{\mathrm{T}}}\ \underset{N\times N}{A}\ \underset{N\times N_B}{W_B}\ \underset{N_B\times 1}{P_B}. \tag{20}$$

If $N = N_B$, P_B can be found by solving the Nth order linear equations in Eq. (19) or (20). If $N > N_B$ or more than one acceleration is measured, the least-squares method can be used to find the time history of the moving forces $P(t)$. If only $N_c (N_c \leqslant N)$ response data points of the beam are used, the equations for these data points in Eq. (20) can be extracted as

$$\underset{N_c\times 1}{\ddot{v}} = \underset{N_c\times N}{(W^*)^{\mathrm{T}}}\ \underset{N\times N}{A}\ \underset{N\times N_B}{W_B}\ \underset{N_B\times 1}{P_B}. \tag{21}$$

In the usual cases, $N_c > N_B$, the least-squares method can be used to find the time history of the moving forces $P(t)$ and more than one acceleration can be used to identify a single moving force for a higher accuracy.

2.3. Identification from bending moments

Similarly, the relationships between bending moment m and its Fourier transform M, and the moving force vector P can be described as follows:

$$\underset{N\times 1}{M} = \frac{1}{N}\underset{N\times N}{B}\ \underset{N\times N_B}{W}\ \underset{N_B\times 1}{P_B}, \tag{22}$$

$$\underset{N\times 1}{m} = \underset{N\times N}{(W^*)^{\mathrm{T}}}\ \underset{N\times N}{B}\ \underset{N\times N_B}{W_B}\ \underset{N_B\times 1}{P_B}, \tag{23}$$

$$\underset{N_c\times 1}{m} = \underset{N_c\times N}{(W^*)^{\mathrm{T}}}\ \underset{N\times N}{B}\ \underset{N\times N_B}{W_B}\ \underset{N_B\times 1}{P_B}. \tag{24}$$

The force vectors P_B can be obtained from the above three sets of equations by using the least-squares method.

2.4. Two forces identification

The above procedures are derived for single-force identification, Eq. (23) can be modified for two force identification using the linear superposition principle as

$$m = (W^*)^{\mathrm{T}}\begin{bmatrix} B_a & 0 \\ B_b & B_a \\ B_c & B_b \end{bmatrix} W_B \begin{Bmatrix} P_1 \\ P_2 \end{Bmatrix}, \tag{25}$$

where $B_a[N_s \times (N_B - 1)]$, $B_b[(N - 1 - 2N_s) \times (N_B - 1)]$ and $B_c[N_s \times (N_B - 1)]$ are sub-matrices of matrix B. The first row of sub-matrices in matrix B describes the state when only the first force on the beam after entry is acting. The second and third rows of sub-matrices describe the states of having two forces on the beam and only one force on the beam after the exit of the first force, respectively. The two moving forces can be identified in a similar manner as before using more than one measured bending moment responses.

2.5. Solutions

As outlined in the previous sections, it is easy to find whether the measured acceleration or bending moment responses are used for moving force identification, the method will usually result in a system of equations that is often of the form

$$Ax = b, \tag{26}$$

where x is the time series vector of the unknown time-varying force $P(t)$, b is the time series vector of the measured bending moment response $m(x, t)$ or of the acceleration response $\ddot{v}(x, t)$ of the bridge deck at the point x and time t. The system matrix A is associated with the system of bridge deck and the force. Its size is of $k \times n$, where k and $n = N_B = L/(c\Delta t)$ are the numbers of data samples for the response $m(x, t)$ or $\ddot{v}(x, t)$ and for the force P, respectively, when the force crosses the whole bridge deck.

The solution we seek corresponds to the optimal solution in terms of the unknown forces, which is equivalent to find the best fit to the given data in a least-squares sense. The optimal

solution is the one that minimizes the norm $\|Ax-b\|^2$. Such a minimization leads to

$$x = A^+ b, \tag{27}$$

where A^+ denotes the PI of matrix A. If A is square and non-singular, then $A^+ = A^{-1}$, and the unknown force vector x can be directly obtained by solving the linear Eq. (26). If A is rectangular ($k > n$) and of full rank, then $A^+ = (A^{\mathrm{T}}A)^{-1}A^{\mathrm{T}}$, the calculation of A^+ presents no problem and the solution x is unique as

$$x = (A^{\mathrm{T}}A)^{-1}A^{\mathrm{T}}b, \tag{28}$$

which is called the (PI) solution.

But often A is rank deficient or nearly rank deficient due to noise or uncertainty in the measured data. In such a situation, x will not be unique. If this is the case, the best way to calculate the PI is via the SVD technique for matrix A [19]. The SVD of an $(k \times n)$ matrix A is a factorization of A into a product of orthogonal matrices

$$U = [u_1, \ldots, u_k] \quad \text{and} \quad V = [v_1, \ldots, v_n]$$

and a diagonal matrix S

$$\underset{k\times n}{A} = \underset{k\times k}{U}\ \underset{k\times n}{S}\ \underset{n\times n}{V^{\mathrm{T}}}, \tag{29}$$

where $S = [\sigma_{ii}]$ is a $(k \times n)$ matrix all of whose entries is zero except for the diagonal elements $\sigma_{ii} = \sigma_i$. The values σ_i are called *singular values* of matrix A and the vectors u_i and v_i are the ith left singular vector (eigenvector of AA^{T}) and the ith right singular vector (eigenvector $A^{\mathrm{T}}A$), respectively. When A is rank deficient, only r singular values are non-zero and they are the positive square roots of the eigenvectors of AA^{T}

$$\sigma_1 \geqslant \sigma_2 \geqslant \cdots \geqslant \sigma_r > 0, \qquad \sigma_{r+1} = \cdots = \sigma_p = 0, \qquad p = \min(k, n).$$

Once the SVD of the matrix A is known, its inverse can easily be calculated below

$$\underset{n\times k}{A^+} = \underset{n\times n}{V}\ \underset{n\times k}{S^+}\ \underset{k\times k}{U^{\mathrm{T}}}. \tag{30}$$

For simplicity, it can be shown that the least-squares solution vector x is given by

$$x = \sum_{i=1}^{r} \frac{u_i^{\mathrm{T}} b_i}{\sigma_i} v_i, \tag{31}$$

which is called the SVD solution in this paper.

3. Experiment in laboratory

In order to validate and evaluate the above identification method, a model car and model bridge deck were made in the laboratory. The car axle spacing to bridge span ratio (ASSR) was set at 0.15 [9]. The model car had two axles at a spacing of 0.55 m and was mounted on four rubber wheels. The static mass of the whole vehicle was 12.1 kg in which the mass of the rear wheel was 3.825 kg. Referring to Fig. 2, the model bridge deck consisted of a main beam, a leading beam and a trailing beam. The leading beam was used to speed up the car so that the car could reach a

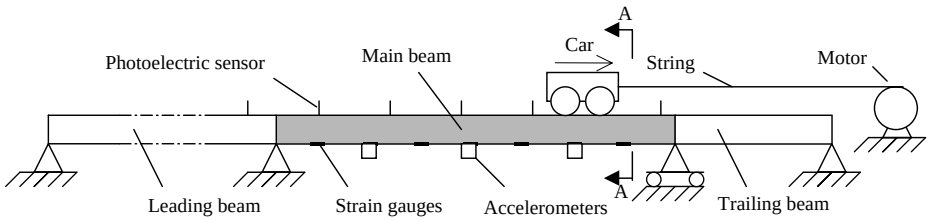

Fig. 2. Experimental set-up of moving force identification.

constant speed when it approaches the main beam. The trailing beam was used for decelerating the car. The main beam, with a span of 3.678 m long and a 101 mm × 25 mm uniform cross-section, was simply supported. It was made from a solid rectangular mild steel bar with a density of 7335 kg/m^3 and a flexural stiffness $EI = 29.97\,\mathrm{kN/m^2}$. The first three theoretical natural frequencies of the main beam bridge were calculated as $f_1 = 4.5\,\mathrm{Hz}, f_2 = 18.6\,\mathrm{Hz}$, and $f_3 = 40.5\,\mathrm{Hz}$.

A U-shaped aluminum track was glued to the upper surface of the main beam as a guide way for the model car, which was pulled along by a string wound around the drive wheel of an electric motor. The speed of the motor could be adjusted. Seven photoelectric sensors were mounted on the beams to measure and check the uniformity of speed of the model car. Seven equally spaced strain gauges and three equally spaced accelerometers were mounted on the lower surface of the main beam to measure the response. A system calibration of the strain gauges was carried out before the actual testing program by adding masses at the middle of the main beam. A 14-channel tape recorder was employed to record the response signals. The first seven channels were used for logging the bending moment response signals from the strain gauges. Channels 8–10 were used for logging the accelerations from the accelerometers. Channel 11 was connected to the photoelectric sensors. In addition, the response signals from channels 1 to 7 and channel 11 were also recorded simultaneously on a PC for easy analysis. The software Global Lab from the Data Translation was used for data acquisition and analysis in the laboratory test. Before exporting the measured data in ASCII format for identification, the Bessel IIR digital filter with low-pass characteristics was implemented as cascaded second order systems. The Nyquist fraction value was chosen to be 0.03.

4. Case studies

In the moving force identification process, many parameters affect the identification accuracy, such as bridge–vehicle system parameters, measurement parameters and algorithm parameters. This case study is aimed to investigate the effects of these parameters on the identification method by comparing the SVD solution in Eq. (31) with the PI solution in Eq. (28).

4.1. Definition of accuracy

In practice, the parameters were studied one at a time. The procedure was to examine each parameter in studied cases and to isolate the case with the highest accuracy for the corresponding

parameter. The accuracy is quantitatively defined as follows, which is called a relative percentage error (RPE).

$$RPE = \frac{\sum |f_{true} - f_{ident}|}{\sum |f_{true}|} \times 100\%. \tag{32}$$

Since the true forces are unknown, Eq. (32) is not practical. The true force (f_{true}) and identified force (f_{ident}) are here replaced by the measured response ($R_{measured}$) and rebuilt response ($R_{rebuilt}$), respectively [9]. Here, the rebuilt responses are calculated from the identified forces using Eq. (26). The RPE values between the measured and rebuilt responses are calculated instead of comparing the identified forces with the true forces directly.

The case study results are only based on the measurements of bending moments in this paper. The identified forces are first calculated from the bending moment responses at all seven measuring stations. The rebuilt responses are then computed accordingly from those identified forces, and the RPE values between the rebuilt and measured bending moment responses at each station are finally examined for validation of the identification method. The maximum acceptable RPE value adopted here is 10% [9]. The results for the measurements of accelerations will be reported separately.

4.2. Effect of tolerence parameter

Usually, the SVD computation is performed in two stages. In the first stage, matrix A is reduced to an upper bidiagonal matrix using the Householder transformation in the following forms:

$$B = \tilde{U}^{\mathrm{T}} A \tilde{V} = \begin{bmatrix} s_1 & e_1 & & & \\ & s_2 & e_2 & 0 & \\ & & \ddots & \ddots & \\ & 0 & & s_{p-1} & e_{p-1} \\ & & & & s_p \end{bmatrix}, \tag{33}$$

where

$$\tilde{U} = U_1 U_2 \cdots U_k, \quad k = \min\{n, m-1\}, \tag{34}$$

$$\tilde{V} = V_1 V_2 \cdots V_l, \quad l = \min\{m, n-2\}. \tag{35}$$

Each transformation matrix U_j ($j = 1, 2, \ldots, k$) sets the elements in rows $j+1$ through m, column j of matrix A to be zero, whereas the matrix V_j ($j = 1, 2, \ldots, l$) sets the elements in columns $j+2$ through n, row j of matrix A to be zero.

The second stage is an iterative process. It applies a variant of the QR algorithm to reduce the super-diagonal elements to a negligible size and to result in a diagonal form through an iteration procedure. If a super-diagonal element e_j satisfies

$$|e_j| \leqslant \varepsilon(|s_{j+1}| + |s_j|), \tag{36}$$

then the element e_j is considered to be zero. Similarly, if a diagonal element s_j satisfies

$$|s_j| \leqslant \varepsilon(|e_{j-1}| + |e_j|) \tag{37}$$

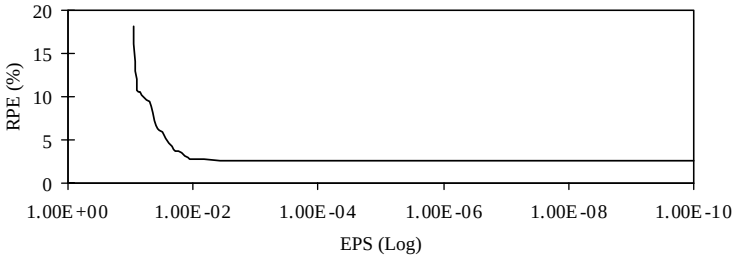

Fig. 3. Effect of tolerance (EPS) used in the SVD technique.

Table 1
Effect of tolerance parameters ε in SVD (15 Unit, $MN = 5$, 250 Hz)

ε	RPE (%)	CPU time (s)	Rank of A
1e−2	2.72	1839.07	1207
1e−3	2.53	1897.73	1207
1e−4	2.52	1920.41	1208
1e−5	2.52	1947.00	1208
1e−6	2.52	1971.28	1208
1e−7	2.52	2001.48	1208
1e−8	2.52	2013.24	1208
1e−10	2.52	2071.41	1208

the element s_j is also considered to be zero, i.e., zero singular value. Here ε is a given tolerance parameter. It is also a criterion related to rejecting or accepting of zero singular values. This criterion may depend on the accuracy of the expected results and, in practice, may be difficult to establish. Fig. 3 shows the effect of the tolerance parameter ε on the identification accuracy (RPE) at the second station. It is observed that a smaller tolerance parameter ε is beneficial to moving force identification and the RPE data are constant if the ε is equal to or smaller than 1e−4. However, if the ε is too small value the computation cost (CPU) is higher. Table 1 shows the detailed effect of the different ε on the RPE, the CPU time and the rank of the matrix A in Eq. (26). To take account of all the above aspects at the same time, the ε value is set to be 1e-6 for all subsequent cases.

4.3. *Effect of measurement parameters*

4.3.1. *Sampling frequencies*

The sampling frequency (f_s) depends on the measurement frequency range of interest. When conducting experiments in the laboratory, the bridge response was acquired at a sampling frequency of 1000 Hz per channel. This frequency is higher than the practical demand because only a few first lower frequency modes are usually used in moving force identification. Sequential data points acquired at 1000 Hz were sampled again at a few intervals in order to obtain new sequential data at a lower sampling frequency. New sequential data at the sampling frequencies of

Table 2
Effect of sampling frequencies (15 Unit, $MN = 5$)

f_s	Sta.1	Sta.2	Sta.3	Sta.4	Sta.5	Sta.6	Sta.7
333	4.51	2.53	1.87	1.95	1.82	2.25	3.17
	204.8[a]	*168.6*	*156.8*	*148.0*	*153.6*	*161.9*	*186.9*
250	4.53	2.52	1.87	1.95	1.82	2.24	3.17
	5.74	*2.80*	*2.15*	*2.08*	*2.14*	*2.41*	*4.74*

[a] Italics data are for the *pseudo-inverse* technique.

333, 250 and 200 Hz would be obtained by sampling the data again at every third, fourth and fifth point, respectively. In the identification, the sampling frequency should be high enough to ensure sufficient accuracy in the discrete integration. However, because there is a computer memory problem in the computation of the inverse of a large matrix, the maximum sampling frequency is limited to be within 500 Hz, the sampling frequencies of 200, 250 and 333 Hz were set here for different MNs involved. The sampling frequency giving the highest accuracy will be adopted for the subsequent studies.

Table 2 shows the effect of the sampling frequency taken into account, in which the RPE values between the measured and rebuilt bending moment are given for the SVD solution and the PI solution, respectively. The case used is for MN which equals to 5, the sensor number is 7 and the vehicle speed is 15 Unit (1 Unit $\cong$ 0.102 m/s). It can be observed from Table 2 that there is an apparent difference in the RPE data by using the SVD and the PI, respectively, particularly at the highest sampling frequency of 333 Hz. When using the PI and the sampling frequency is 333 Hz, the identification method failed since none of the RPE data at seven stations are acceptable and higher than 148%. But the identification accuracy increases with decrease in the sampling frequency. When decreasing the sampling frequency to 250 Hz, the identified results are in the acceptable range. This shows that the identification method is suitable for a lower sampling frequency when the PI is used to solve the equation. Significantly, the SVD identified results are clearly different from those found by PI. They are almost constant at each station for the different sampling frequencies. This means that the identification method is independent of the sampling frequency when adopting the SVD. The SVD can effectively improve the identification accuracy especially when the sampling frequency is of the highest value of 333 Hz. The use of the SVD not only makes the identification method effective but also results in good identified results with higher accuracy, whereas direct calculation of the PI solution causes the identification method to fail.

Evaluating the identified results further, Fig. 4 also compares two moving forces identified by the SVD and PI methods, respectively, under different sampling frequencies. When $f_s = 250$ Hz, obviously, the PI results become much worse as there are many higher frequency components in the identified forces, whereas the SVD curve remains almost unchanged. When $f_s = 333$ Hz, the identification method fails if the PI is adopted, but the identification method is effective and results in almost the same good as the previous cases if the SVD is adopted. Fig. 4 illustrates the PI method is effective only under the lower sampling frequencies, while the identification method consistently achieved good identification accuracy when the SVD is adopted at different sampling frequencies.

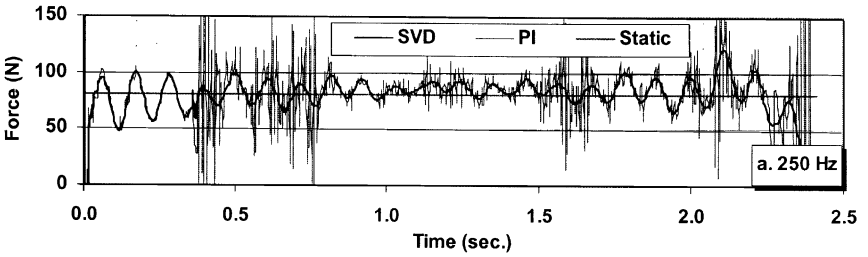

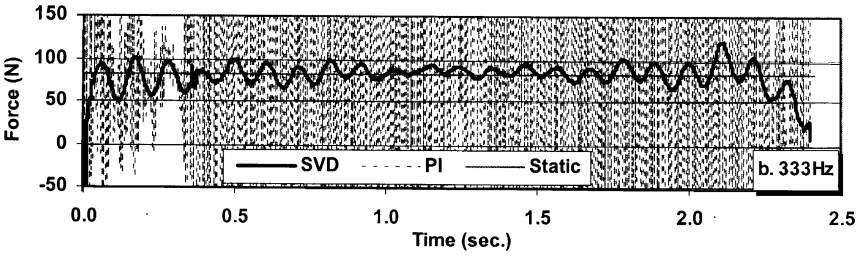

(4.1) Identified loads at first axle

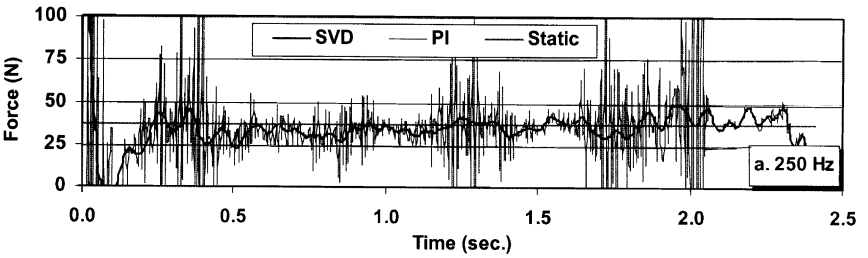

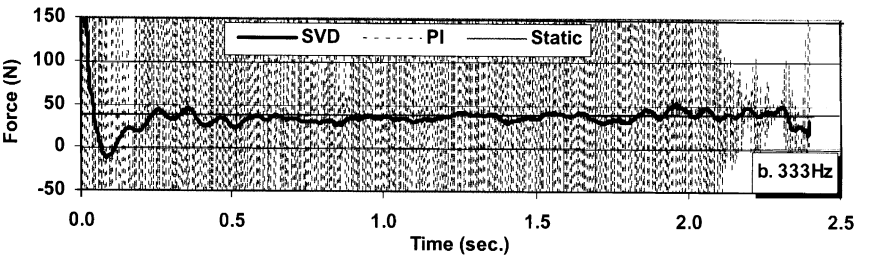

(4.2) Identified loads at second axle

Fig. 4. Effect of sampling frequencies (15 Unit, $MN = 5$).

There include higher frequency components, i.e., more perturbation in the system matrix A in Eq. (26) when the sampling frequency is higher. Elements of PI matrices are sensitive to those small perturbations in the data, say ill-conditioned problem, when the PI method is adopted [20]. However, the SVD overcomes the problem by setting very small singular values to zero in the inverse matrix [18]. Therefore, the SVD solution is stable but the PI solution varies clearly with the sampling frequency.

Table 3
Effect of measuring stations (15 Unit, 250 Hz)

Station	RPE (%)							
	No. = 3		No. = 4		No. = 5		No. = 7	
1	[a]		[a]		[a]		4.53	*5.74*
2	[a]		1.67	*2.90*[b]	2.14	*34.63*	2.52	*2.80*
3	1.24	*70.15*	1.50	*2.09*	1.71	*17.25*	1.87	*2.15*
4	1.38	*77.27*	[a]		1.77	*34.68*	1.95	*2.08*
5	1.05	*73.90*	1.51	*2.11*	1.71	*16.65*	1.81	*2.14*
6	[a]		1.68	*2.74*	1.63	*32.87*	2.24	*2.41*
7	[a]		[a]		[a]		3.17	*4.74*

[a] Indicates the station is not chosen.
[b] Italics data are for the *pseudo-inverse* technique.

4.3.2. Measurement stations

If parameters $MN = 5$, $f_s = 250$ Hz, $c = 15$ Unit are not changed, measurement station numbers (*No.*) are set to be 2, 3, 4, 5, and 7, respectively, for all study cases in this section. The RPE data between the rebuilt and measured responses are given in Table 3 when using the SVD and the PI to solve the equations in the identification method. Here, the RPE data for the case *No.* = 2 are not listed because the identification method fails for both solution techniques. It shows that the identification method adopted to identify two moving forces requires at least three measurement stations whichever solution technique is used to solve the equations.

When using the PI and the *No.* = 3, the underlined RPE data in Table 3 show that the identification method failed to correctly identify the two moving forces. However, if there is an increase by one more measurement station, i.e., *No.* = 4, the RPE data dramatically fall into the acceptable range and are at a very low level of less than 3% at each one of the four stations. Unfortunately, if *No.* = 5, the RPE data obviously increase and are unacceptable. On studying the location of the additional fifth station, it is found that the fifth station is on the half span point, which is the node of the second and fourth modes of the supported beam. This makes the PI solution unstable and makes the identification method ineffective. Nevertheless, when *No.* = 7, i.e., two more stations are added at the $\frac{1}{8}$ span and $\frac{7}{8}$ span, respectively, the RPE data recover to normal acceptable levels to within 10%. These indicate that the identification method is very sensitive to the locations of the measuring stations when the PI is used. Selection of measurement stations should be taken therefore, with care.

Once the SVD is used in the identification method, the RPE data in Table 3 show that the identified results are acceptable and achieve a very high accuracy for all the study cases in this section. In particularly, the RPE data are less than 2.53% at the middle five stations. It is also predicted that the identification method is independent of the measurement stations if the SVD method is adopted. Further, Fig. 5 illustrates a comparison between the identified first axle forces and the identified second axle forces when changing measurement stations. Obviously, the identified results are getting better and better with an increase in the number of measurement stations. The best result corresponds to the case with the most measurement stations *No.* = 7. The others are also acceptable except for the case with *No.* = 3. The two dynamic moving forces vary

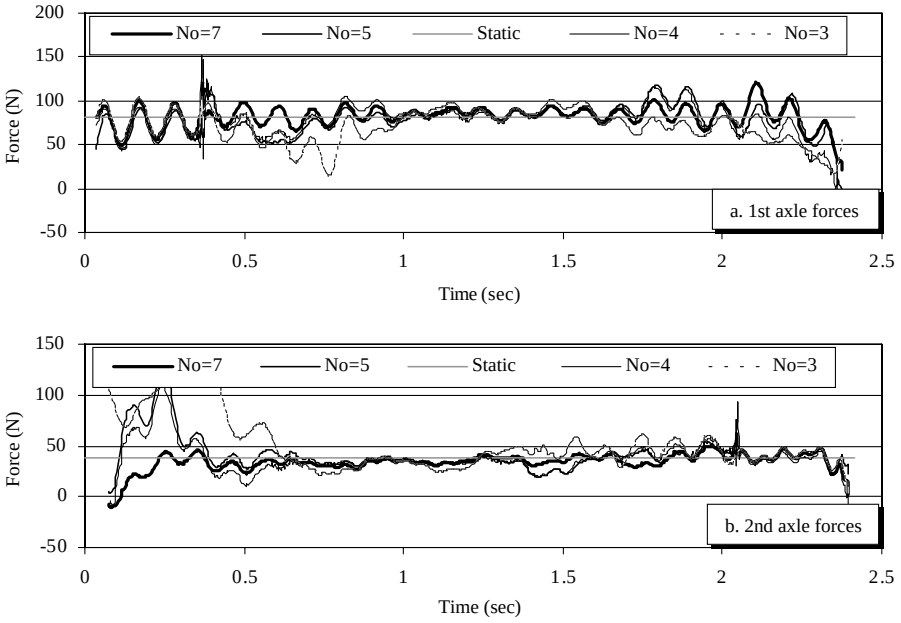

Fig. 5. Effect of measurement stations when using the SVD ($MN = 5$ and 250 Hz).

about the static weight line of vehicle axles. It is credible and feasible, especially when the two axles are on the bridge.

4.4. *Effect of bridge–vehicle system parameters*

4.4.1. *Bridge MNs*

Usually, in a moving force identification system, a sufficient number of vibration modes of bridge must be included in the identification calculation. But what is the sufficient number of modes? The answer depends not only upon the characteristics of the bridge–vehicle system but also upon the solution to the overdetermined equation used in the moving force identification method. In this section, MNs varied from $MN = 1$ to 5. The case $f_s = 250$ Hz and $c = 15$ Unit was chosen for detailed examination. If the MNs are less than three, the RPE values are very high and the identified forces become unacceptably inaccurate, and the identification method fails to identify the two moving forces caused by the vehicle crossing the bridge. However, if the MNs are equal to or bigger than three, the RPE data move into an acceptable range as listed in Table 4. This shows the identification method is effective only if a sufficient number of modes is achieved or exceeded, otherwise the method fails. Studying the RPE data in Table 4 more carefully, when the RPE data at all seven stations are acceptable, a sufficient number of modes are four for the use of the SVD, but five for the use of the PI.

Table 4 also shows that the RPE data decrease slightly with an increase in the MN whether using the SVD or the PI. Further, comparing the RPE data at each station, it can be found that the RPE data using the SVD are clearly improved, particularly for the lower MN cases $MN = 3$

Table 4
Effect of MNs (15 Unit, 250 Hz)

MN	RPE (%)						
	Sta. 1	Sta. 2	Sta. 3	Sta. 4	Sta. 5	Sta. 6	Sta. 7
3	12.10	3.51	5.26	2.61	5.21	3.70	12.91
	Fail[a]	*Fail*	*Fail*	*Fail*	*Fail*	*Fail*	*Fail*
4	5.88	3.24	2.03	2.64	1.97	3.55	5.83
	13.58	*7.19*	*5.69*	*5.93*	*5.55*	*6.75*	*12.91*
5	4.53	2.52	1.87	1.95	1.81	2.24	3.17
	5.74	*2.80*	*2.15*	*2.08*	*2.14*	*2.41*	*4.74*

[a] Italics data are for the *pseudo-inverse* technique.

and 4. When $MN = 3$ and using the PI, the method fails, but using the SVD the identified results are acceptable except the RPE values at the 1st and 7th stations. When $MN = 4$, use of the SVD effectively reduces the RPE data at each station about 60% more than those using the PI. It shows that using the SVD to solve the system equation can effectively improve the identification accuracy. Fig. 6 also shows the identified forces for $MN = 4$ and 5 when the SVD and the PI are, respectively, used in the identification method.

The PI curves in Fig. 6 are apparently worse than the SVD curves because they have components with higher frequency noise. Fortunately, the identified forces are clearly getting better and better with increase in the MN especially for the PI method. The scatter in the magnitudes of forces identified by the PI is apparently reduced with increase in MN. Although increase in MN is also beneficial to the SVD approach, the improvement is not so obvious as with the PI approach. Fig. 7 shows the forces identified by the SVD when $MN = 4$ and 5. It clearly illustrates that when increasing MN the improvement of the identified forces is mainly focused on about 0.365 s for the first force, i.e., the moment when the second wheel approaches the bridge, and located before 0.365 s for the second force. When both vehicle wheels are on the bridge, the identified forces are independent of change in MN. This indicates use of the SVD is not so sensitive to a change in MN.

When the MN is equal to five, the RPE data in Table 4 show that the identified forces are acceptable whether using the SVD or the PI. As an example, the corresponding rebuilt responses are compared in Fig. 8. The curves in Fig. 8 illustrate that both the SVD and the PI are feasible and in a good agreement with the measured responses except there are obvious discrepancies in a few small intervals. Of course, as for the comments on the identified forces, the rebuilt responses due to the SVD are matched better than that due to the PI. It can be seen that although the latter also matches with the measured responses in the trend its curves show many jumps, i.e., higher frequency noise.

4.4.2. *Vehicle speeds*

If bridge MNs, sampling frequencies and bridge span length are not changed, changes in vehicle speeds would mean changes in data samples, i.e., changes in the size of coefficient matrix $\boldsymbol{A}$ in Eq. (26). Some limitations on the identification method have been considered. In particular, a

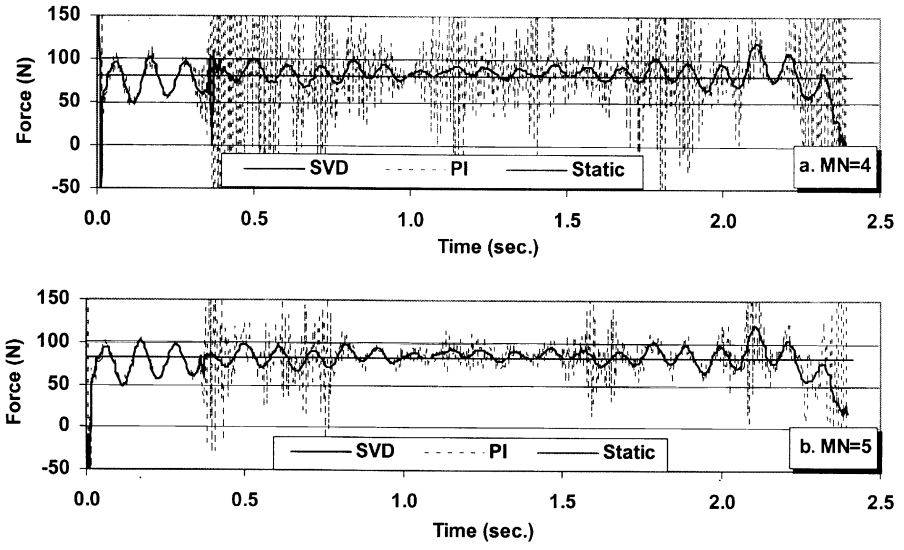

(6.1) Identified loads at first axle

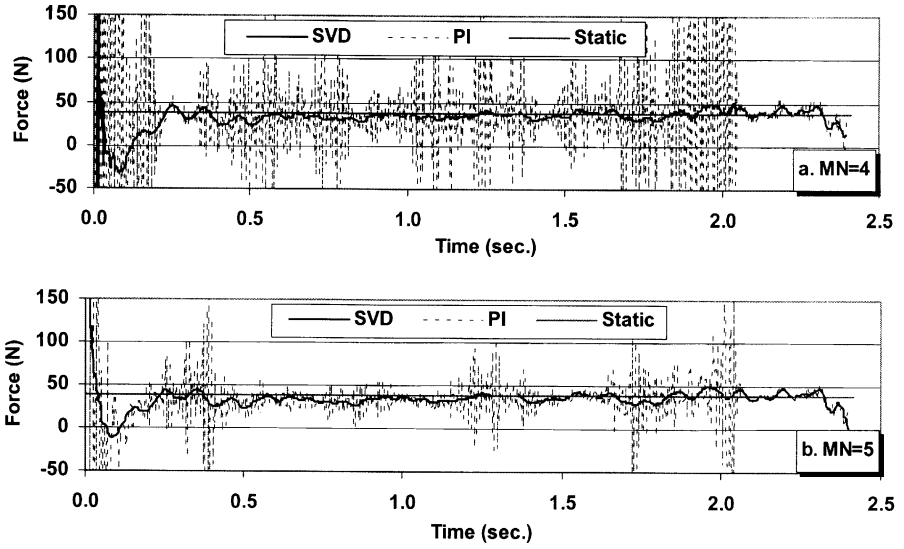

(6.2) Identified loads at second axle

Fig. 6. Effect of MNs (250 Hz and 15 Units).

minimum necessary RAM memory and personal computer CPU speed are required for the method. Otherwise, calculation will take a significant amount of execution time due to the large size of matrix A, or they might not be capable of being performed at all due to insufficient memory. Therefore, in order to make the identification method effective and to properly evaluate

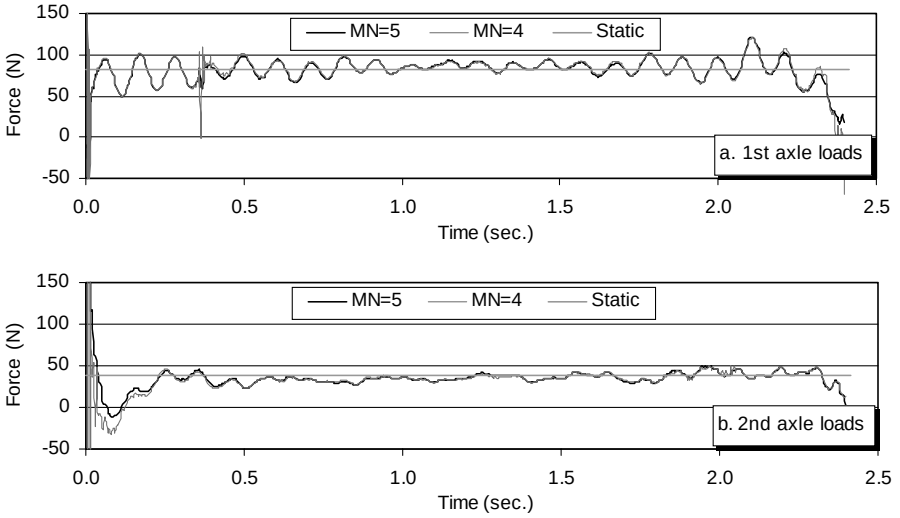

Fig. 7. Effect of MNs when using the SVD (250 Hz and 15 Units).

the effects of various vehicle speeds on the identified results, the case with $MN = 4$, $f_s = 200$ Hz was selected for this section.

While conducting the experiments in the laboratory, three vehicle speeds were set manually at 5, 10 and 15 Unit, respectively. In order to make vehicle speed as constant as possible when the vehicle moved across the main beam, some measures were taken in the experiments. For instance, a sufficiently long leading-beam was placed in front of the test main beam to enable the vehicle to reach a constant speed by the time it reaches the main beam. Using a sufficiently stiff string to take the vehicle can also reduce the effects of string elastic deformation on the vehicle speed. After acquiring the data, the vehicle speed was calculated and the uniformity of speed checked. If the speed was stable, the experiment was repeated five times for each speed case to check whether or not the properties of the structure and the measurement system had changed. If no significant change was found, the corresponding recorded data was accepted for moving force identification. After checking the vehicle speed between two triggers, it was found that apparent differences in the speed existed in different segments of the main beam, but the variation was within an acceptable error level. However, the average speed of the vehicle on the whole beam was used to identify the moving forces in the calculation.

The RPE data are calculated and tabulated in Table 5 for cases 5-2, 10-4 and 15-2, where, case "5-2" means the *second set* of data was recorded when the vehicle moved across the bridge at a speed of 5 Unit. Others are similarly identified. Table 5 shows that the RPE data decrease with increase in vehicle speeds whether for the SVD or for the PI. For the PI approach, the identification method fails to identify the two moving forces when the vehicle speed is lower, say 5 Unit, but the identified results are getting better and better as the vehicle speed increases. Fortunately, the identified result is acceptable at last in the case of 15 Unit. However, when using the SVD approach the situation is completely changed. When the speed is 5 Unit, the originally ineffective identification method becomes effective although the RPE data at the two end stations

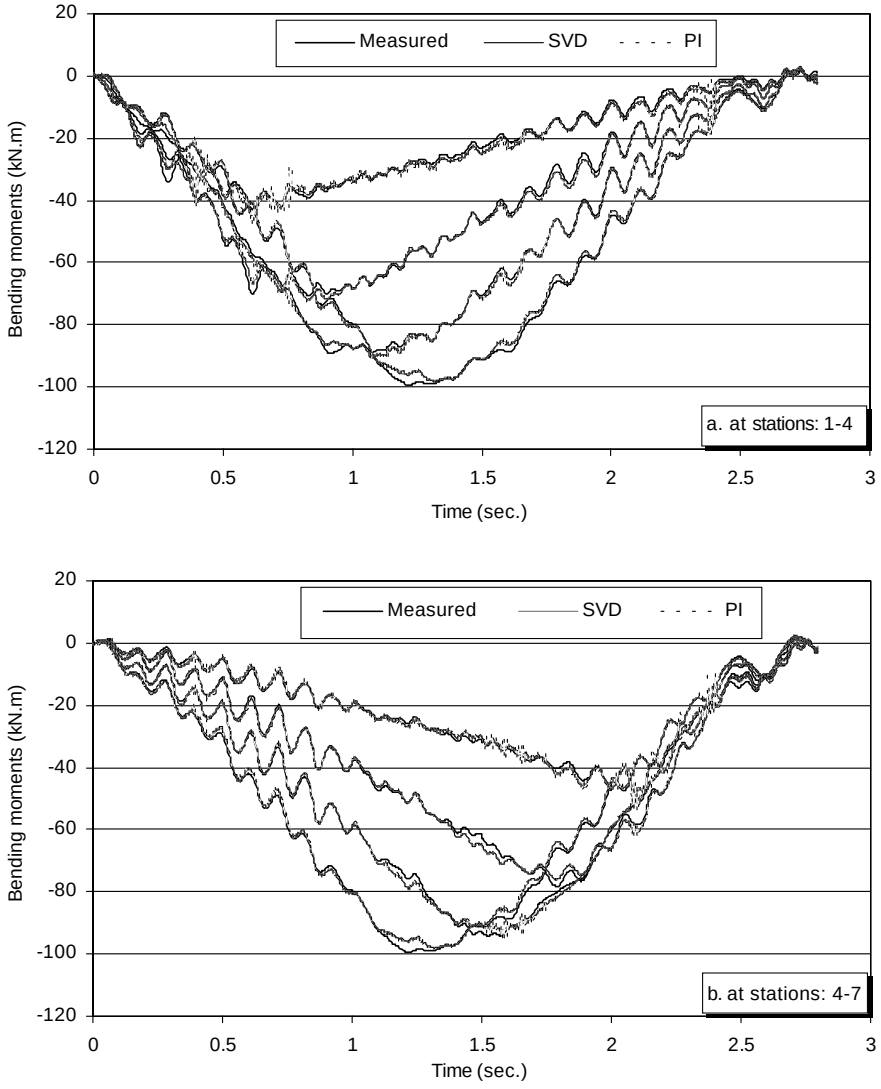

Fig. 8. Comparison of responses ($MN = 5$, 250 Hz and 15 Unit).

are higher than 10%. The originally more significant RPE data become small when the speed is 10 Unit. When the vehicle moves at 15 Unit the identification accuracy is also a little improved and a little better than that due to the PI approach although both sets of RPE data are very close to each other. Fig. 9 illustrates a comparison of the responses at station 4 under three different vehicle speeds. It indicates that a proper solution to a set of equations plays a very important role in moving force identification. It is better to use the SVD to solve the system equation so that the identification method can be effective and can identify the two moving forces with a higher accuracy. These results also show that the identification accuracy for the faster vehicle speeds is greater than for the lower vehicle speed whether the SVD or the PI approach is used.

Table 5
Effect of vehicle speeds ($MN = 4, f_s = 200$ Hz)

Station	RPE (%)					
	5–2		10–4		15–2	
1	23.71	*Fail*	23.3	*110.0*[a]	5.87	*5.94*
2	13.00	*Fail*	12.6	*50.0*	3.24	*3.29*
3	6.79	*Fail*	7.99	*25.9*	2.04	*2.05*
4	7.90	*Fail*	8.32	*48.2*	2.65	*2.66*
5	6.93	*Fail*	7.79	*24.8*	1.98	*2.01*
6	12.40	*Fail*	11.8	*47.6*	3.55	*3.57*
7	26.37	*Fail*	26.3	*102.*	5.84	*5.89*

[a] Italics data are for the *pseudo-inverse* technique.

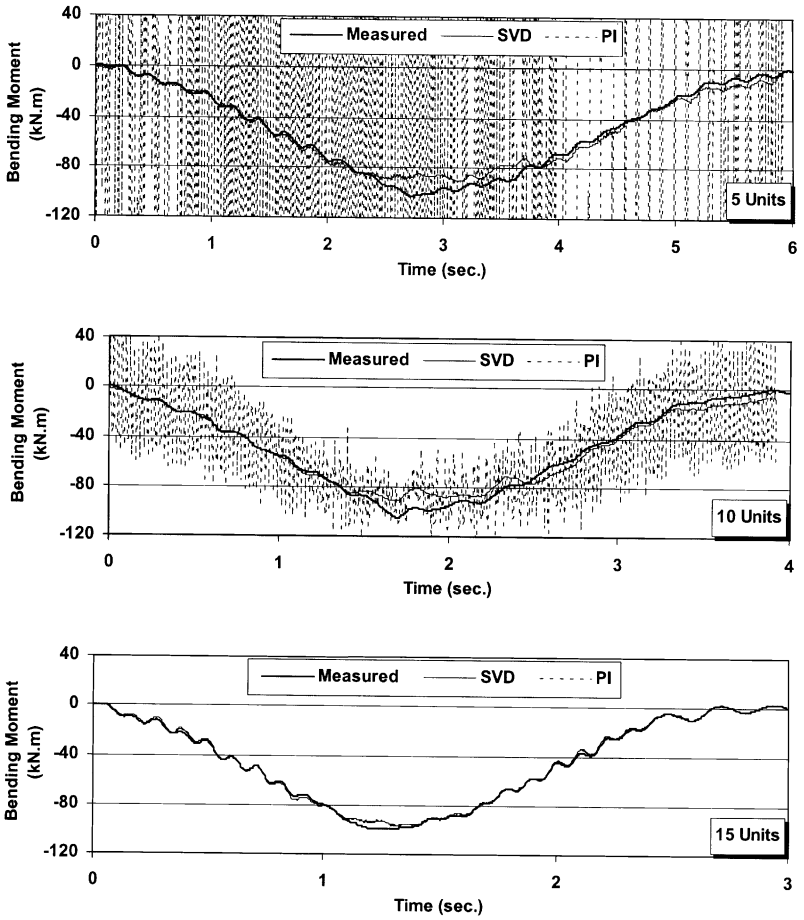

Fig. 9. Comparison of responses at station 4 under different speeds ($MN = 4$ and 200 Hz).

5. Conclusion

The frequency–time domain method is used in this paper to identify the axle force history of a moving vehicle on a bridge. A bridge–vehicle system model is made in the laboratory for moving force identification. A series of experiments on bridge responses caused by the vehicle moving across the bridge are conducted. Case studies on moving force identification are carried out. The effects of parameters, such as bridge–vehicle system parameters, measurement parameters and tolerance parameter used in the singular value decomposition (SVD), are investigated. Emphasis has been placed on a comparison between the SVD solution and the pseudo-inverse (PI) solution adopted in the identification method. The following conclusions are drawn: (1) a moving force identification method is often converted into the solution of a set of overdetermined equations. The solution plays a very important role in moving force identification. It is vital to understand whether the identification method is likely to be successful or not. (2) When the PI solution is adopted to solve the overdetermined equations, the method can effectively identify two moving forces in some situations, but it sometimes fails. The PI solution is sensitive to changes in various parameters and the identified results are often unstable. (3) In contrast, if the SVD solution is adopted, the method not only effectively identifies the two axle moving forces with a higher accuracy but also gives stable and reliable results. The identification method is almost independent of changes in parameters. (4) The identified results from the use of the SVD solution in the identification method are therefore better than those found by direct calculation of the PI solution. The SVD solution, as the more practical approach, should be incorporated into the moving force identification system. (5) The great drawback of using the SVD explicitly is its computation cost. For instance, it increases by about 60% for the case studies when compared to that for the PI. It is not beneficial to the real-time analysis on site. Performing a full-SVD could be too expensive in practical applications since the size $(k \times n)$ of matrix A in Eq. (26) may be extremely large. In these cases, algorithm to compute a partial SVD could be used [21]. Another possibility is to replace the full-SVD by a RRQR factorization, which can save substantially computational effort [20].

Acknowledgements

Funding support to the project from the Research Grants Council of the Hong Kong SAR Government (Polyu 5086 197E) is gratefully acknowledged.

References

[1] K.K. Stevens, Force identification problems—an overview, Proceedings of SEM Spring Conference on Experimental Mechanics, Florida, 1987, pp. 838–844.

[2] B.J. Dobson, E. Rider, A review of the indirect calculation of excitation forces from measured structural response data, Proceedings of the Institution of Mechanical Engineers, Part C: Journal of Mechanical Engineering Science 204 (1990) 69–75.

[3] L. Fryba, Vibration of Solids and Structure Under Moving Loads, Noordhoff International Publishing, Groningen, 1972.

[4] S.P. Timoshenko, D.H. Young, W. Weaver, Vibration Problems in Engineering, Wiley, New York, 1974.
[5] T.H.T. Chan, C. O'Connor, Wheel loads from highway bridge strains: field studies, Journal of Structural Engineering, American Society of Civil Engineers 116 (1990) 1751–1771.
[6] S.S. Law, T.H.T. Chan, Q.H. Zeng, Moving force identification: a time domain method, Journal of Sound and Vibration 201 (1997) 1–22.
[7] S.S. Law, T.H.T. Chan, Q.H. Zeng, Moving force identification-a frequency and time domain analysis, Journal of Dynamic System, Measurement and Control 121 (1999) 394–401.
[8] T.H.T. Chan, S.S. Law, T.H. Yung, X.R. Yuan, An interpretive method for moving force identification, Journal of Sound and Vibration 219 (1999) 503–524.
[9] T.H.T. Chan, L. Yu, S.S. Law, Comparative studies on moving force identification from bridge strains in laboratory, Journal of Sound and Vibration 235 (1) (2000) 87–104.
[10] T.H.T. Chan, L. Yu, S.S. Law, T.H. Yung, Moving force identification studies, I: theory, Journal of Sound and Vibration 247 (1) (2001) 59–76.
[11] T.H.T. Chan, L. Yu, S.S. Law, T.H. Yung, Moving force identification studies, II: comparative studies, Journal of Sound and Vibration 247 (1) (2001) 77–95.
[12] J.A. Fabunmi, Effects of structural modes on vibratory force determination by the pseudo-inverse technique, American Institute of Aeronautics and Astronautics 24 (1986) 504–509.
[13] L. Yu, T.H.T. Chan, Moving force identification from bending moment responses of bridges Structural Engineering and Mechanics, An International Journal 14 (2) (2002) 151–170.
[14] S. Hashemi, J.K. Hammond, The interpretation of singular values in the inversion of minimum and non-minimum phase systems, Mechanical Systems and Signal Processing 10 (3) (1996) 225–240.
[15] H. Gloub, W. Kahan, Calculating the singular values and pseudo-inverse of a matrix, SIAM Journal of Numerical Analysis Series B. 2 (1965) 48–59.
[16] T.F. Chan, An improved algorithm for computing the singular value decomposition, ACM Transactions on Mathematical Software 8 (1982) 72–83.
[17] J.A. Brandon, C.F. Cremona, Singular value decomposition: sufficient but not necessary, Proceedings of Eighth International Modal Analysis Conference, Florida, Vol. 2 (1990) 1376-1380.
[18] W.H. Press, S.A. Teukolsky, W.T. Vetteling, B.P. Flannery, Numerical Recipes in Fortran 90: The Art of Parallel Scientific Computing, 2nd Edition, Vol. 2, Fortran Numerical Recipes, Cambridge University Press, Cambridge, 1996.
[19] G. Lindfield, J. Penny, Numerical Methods Using Matlab, Ellis Horwood, London, 1995.
[20] F.S.V. Bazan, C.A. Bavaseri, An optimized pseudo-inverse algorithm (OPIA) for multi-input multi-output modal parameter identification, Mechanical Systems and Signal Processing 10 (4) (1996) 365–380.
[21] C.R. Vogel, J.G. Wade, Iterative SVD-based methods for ill-posed problems, SIAM Journal on Scientific Computing 15 (1994) 736–754.